



# Evaluation of near immersion active cooling on the microstructure and mechanical properties of AISI 316L stainless steel obtained with additive manufacturing by DED-Arc

Julia Nascimento Costa<sup>1</sup> · Geovane de Assis Faria<sup>3</sup> · Rodrigo Rangel Porcaro<sup>1</sup> · Igor César Pereira<sup>2</sup>

Received: 9 February 2024 / Accepted: 24 July 2024 / Published online: 3 August 2024  
© The Author(s), under exclusive licence to Springer-Verlag London Ltd., part of Springer Nature 2024

## Abstract

The directed energy deposition arc (DED-Arc) has been extensively used to develop metallic parts with varying complexities. A major challenge for austenitic stainless steels is managing heat accumulation due to their low thermal conductivity. This study aimed to characterize the microstructure and mechanical properties of AISI 316L preforms manufactured by additive manufacturing (AM) under different deposition paths and cooling conditions. Samples underwent macro- and microstructural analyses, and tensile and hardness tests to evaluate their mechanical behavior. Additionally, the effect of active cooling using near immersion active cooling (NIAC) in water on the microstructure was assessed by examining the secondary interdendritic spacing and ferritic phase fraction. The NIAC technique has shown potential for enhancing productivity by producing preforms with more uniform thickness and consistent solidification/cooling conditions throughout the multiple layers. This approach eliminated deposition idle time, leading to a productivity increase of up to 108%. Microstructures obtained with active cooling were more refined than those resulting from natural cooling, evidenced by a reduction in secondary interdendritic spacing and an increased fraction of delta ferrite. These microstructural changes resulted in higher hardness and mechanical strength in the material processed with the NIAC technique. However, difficulties in precisely controlling the water level resulted in increased apparent porosity when using the NIAC technique.

**Keywords** Additive manufacture · Near immersion active cooling · AISI 316L · Stainless steel · Wire arc additive manufacturing

## 1 Introduction

Wire and arc-based additive manufacturing is a promising technology for building large-scale and highly individualized metallic components [1]. According to the ASTM Standard [2], this process is referred to as directed energy deposition (DED-Arc) when an electric arc is used as the power source.

Although DED-Arc has several advantages over the powder-bed fusion process—such as higher deposition rate, lower material costs when using wire form, and the simplicity of the welding process compared to lasers and electron beams [3]—it also has some limitations. The significant heat input and the serious thermal accumulation can affect precision and limit the suitability of these processes [1, 3–5].

In a recent paper, Reisgen et al. [1] reviewed cooling strategies to enhance the efficiency of DED-Arc during additive manufacturing. The authors emphasized that to maintain competitiveness, higher manufacturing speeds are essential when dealing with lower-cost (metallic) materials. The manufacturing speed is determined by the deposition rate of the welding process and the idle time required for the workpiece to cool down to the required interpass temperature [1, 5]. The interpass temperature and cooling rate influence solidification behavior, grain growth, and phase transformation [1].

✉ Rodrigo Rangel Porcaro  
rodrigo.porcaro@ufop.edu.br

<sup>1</sup> Rede Temática em Engenharia de Materiais (REDEMAT), Universidade Federal de Ouro Preto (UFOP), Ouro Preto, MG, Brazil

<sup>2</sup> Programa de Pós-Graduação em Engenharia Mecânica (PROPEM), Universidade Federal de Ouro Preto (UFOP), Ouro Preto, MG, Brazil

<sup>3</sup> Departamento de Engenharia Metalúrgica e de Materiais (DEMET), Universidade Federal de Ouro Preto (UFOP), Ouro Preto, MG, Brazil

Da Silva et al. [5] developed an active cooling strategy based on a water batch, named near immersion active cooling (NIAC). This recent development has been applied to a limited number of materials up to now, but shows a promising alternative to produce large components with controlled thermal parameters [6, 7].

Stainless steels are favorable candidates for DED-Arc due to their good mechanical properties and high corrosion resistance [5]. The austenitic stainless steel AISI 316L, in particular, has been extensively studied and applied in additive manufacturing because of its reliable mechanical properties and corrosion resistance for a wide range of processing variables. Cunningham et al. [8] emphasize the importance of knowing the processing-microstructure-properties relationship for this material. Moreover, austenitic stainless steels have lower thermal conductivity than ferritic or carbon steels, which imposes additional challenges related to thermal control during DED-Arc [9].

The 316L stainless steel exhibits a duplex microstructure after being processed by DED-Arc [7–9]. The aspects related to solidification and solid-phase transformation result in various microstructural features, such as the amount of delta ferrite and the average secondary dendrite arm spacing, among others [8, 10]. Jafarzad-Shayan et al. [9] concluded that the relatively high solidification and cooling rates during DED-Arc are responsible for increasing the amount of delta ferrite in 316L stainless steel. The authors [9] also found that lower cooling rates at the top of deposited material resulted in a lower amount of delta ferrite [6.1%] compared to the base [8.6%], due to heat accumulation along the height of the obtained preforms.

In the absence of information regarding the effects of NIAC on the productivity, microstructures, and properties of the 316L stainless steel, this work was developed. Preforms, consisting of simple geometry of thin walls, were obtained using DED-Arc (gas metal arc welding (GMAW)), both with and without the application of active cooling (NIAC). The microstructure and the conventional mechanical properties, specifically hardness and tensile strength, were assessed in different sections of the thin walls. The results demonstrated that thermal management through NIAC is a promising approach for the additive manufacturing of this austenitic stainless steel. The microstructure and mechanical properties were found to be significantly sensitive to variations in the cooling rate. Specifically, active cooling resulted in a reduction of up to 38% in secondary interdendritic arm spacing, associated with an increase of up to 108% in productivity.

## 2 Materials and methods

As depicted in Fig. 1, the experimental work involved the fabrication and characterization of preforms using AISI 316L stainless steel, both with and without active cooling by NIAC. The primary objective was to compare productivity (manufacturing time), precision (geometry), and microstructural

and mechanical properties. Additionally, we evaluated the effects of different paths during the manufacture on the preforms, which will be detailed in the following sections.

### 2.1 Materials

For this study, AISI 316LSi stainless steel was used in the form of a 1.0-mm-diameter wire electrode for the electric arc deposition process. A low-carbon steel plate (AISI 1020) was selected as the base for manufacturing, with the initial layers discarded to prevent dilution. Argon with 99.99% purity served as the shielding gas. The chemical composition of AISI 316LSi steel can be found in Table 1.

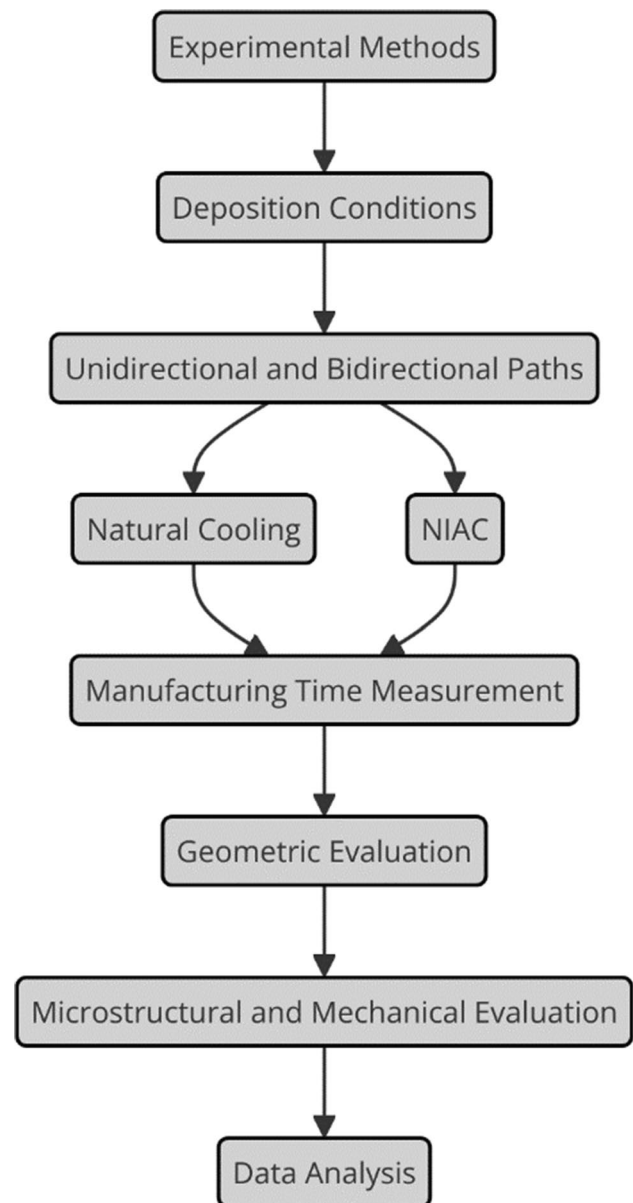


Fig. 1 Flowchart depicting the main steps undertaken in this study

**Table 1** Chemical composition for AISI 316LSi steel

| Element | C    | Cr        | Ni        | Mo      | Mn  | Si   | P     | S    | N   |
|---------|------|-----------|-----------|---------|-----|------|-------|------|-----|
| WT %    | 0.03 | 16.0–18.0 | 10.0–14.0 | 2.0–3.0 | 2.0 | 0.75 | 0.045 | 0.03 | 0.1 |

### 2.2 Experimental methods

The study was divided into four comparative deposition conditions, as shown in Table 2.

For both approaches, with and without active cooling, a GMAW welding source was employed for material deposition and geometry construction. The torch was automatically manipulated, and the geometry constructed (X, Y, and Z movements) using a D600 Romi machining center head programmed via computer numerical control (CNC).

The welding process parameters influencing heat input (voltage, current, and torch movement speed) were determined based on wire diameter, preliminary tests, and data from the literature. The specific trial conditions are detailed in Table 3.

For NIAC I and NIAC II depositions (Table 2), the near immersion active cooling (NIAC) technique was employed. In this setup, the carbon steel base was positioned inside a water vat, with the liquid level adjusted to increase as the height of the built wall progressed, as illustrated in Fig. 2.

To control the water level in the tank, two flow meters were utilized—one at the inlet and another at the outlet of the container. The objective was to regulate the water inflow into the tank, ensuring it exceeded the outflow to guarantee, in addition to water recirculation, the increase in the level inside the water vat, in a controlled and synchronized way with the deposition process.

The manufacturing times of the four deposition conditions were recorded. The manufacturing time of the wall encompasses the total time spent in fabrication—from the initial activation of the timer until the completion of the deposition of the last layer of material. This includes the return time of the torch to its initial position in unidirectional depositions, as well as the idle cooling time accounted for Air I and Air II conditions, where natural cooling was applied.

**Table 3** Welding parameters used in the manufacture of AISI 316LSi austenitic stainless steel preforms (thin walls)

|                        |        |
|------------------------|--------|
| Current                | 140 A  |
| Torch speed            | 4 mm/s |
| Tension                | ~20 V  |
| Distance pool-torch    | 12 mm  |
| Length of the preforms | 120 mm |

The variable real deposition time was obtained by counting only the time during which material deposition occurred in the construction of the preforms. Efficiency was defined as the ratio of actual deposition time to the total manufacturing time of the wall and is calculated using Eq. 1.

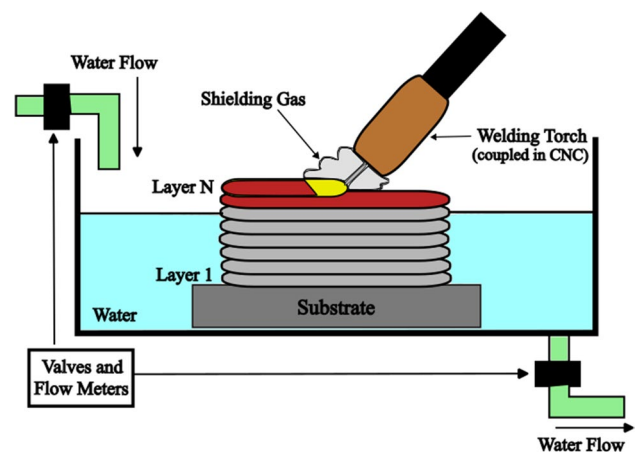


**Fig. 2** Schematic representation of NIAC (near immersion active cooling) setup

**Table 2** Deposition conditions for the construction of preforms (thin walls)

| Condition | Method/path    | Cooling         | Identification | Deposition details   |
|-----------|----------------|-----------------|----------------|--|
| I         | Unidirectional | Natural cooling | Air I          | Deposition of 10 consecutive unidirectional passes with an idle cooling time <sup>1</sup> before commencing new depositions, reaching a total of 20 layers |
| II        | Bidirectional  | Natural cooling | Air II         | Deposition of 4 consecutive bidirectional passes with an idle cooling time <sup>1</sup> before commencing new depositions, reaching a total of 20 layers   |
| III       | Unidirectional | NIAC            | NIAC I         | Deposition of 20 consecutive unidirectional layers   |
| IV        | Bidirectional  | NIAC            | NIAC II        | Deposition of 20 consecutive bidirectional layers  |

<sup>1</sup>The number of consecutive passes was determined by previous tests in both conditions. The idle time was defined as the time enough to the center of the last pass reaching 200 °C (interpass temperature), using a K-type thermocouple in contact with the surface

$$\text{Efficiency (\%)} = \frac{\text{Real-time deposition}}{\text{Preforms manufacturing time}} \times 100 \quad (1)$$

The productivity increase with NIAC was determined using Eq. 2, taking into account both deposition paths:

$$\text{Productivity increase with NIAC (\%)} = \left[ \left( \frac{\text{Efficiency with NIAC (\%)}}{\text{Efficiency with natural cooling (\%)}} \right) - 1 \right] \times 100 \quad (2)$$

To evaluate the geometry of walls manufactured (preforms) by additive manufacturing, the height and thickness of the parts at the sides and center of the walls were analyzed and compared. Additionally, the thicknesses of the walls were measured (Fig. 3).

For microstructural evaluation, the central portion of the wall was selected with a longitudinal analysis plane, as depicted in Fig. 3. Samples were cut, sanded, polished, and etched using electrochemical etching with oxalic acid ( $\text{C}_2\text{H}_2\text{O}_4$ ).

The metallographic analyses were conducted at the base, center, and top regions of the deposited wall. To

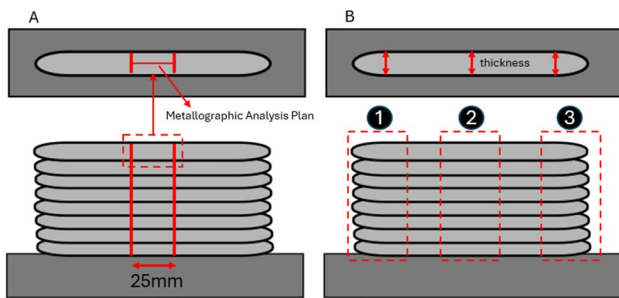
avoid the regions affected by reheating or layer transitions, all qualitative and quantitative metallographic analyses were performed on the central areas of the layers at each respective position, as exemplified in Fig. 4.

From the images obtained through optical microscopy, the secondary interdendritic arm spacing (SDAS) was analyzed using the method identified by Vandersluis and Ravindran [11] as having the lowest associated error. SDAS was measured in images with  $200\times$  magnification using the ImageJ software. This linear interception method, which involves counting the secondary arms that intersect a line drawn parallel to a primary dendrite arm, was employed, as illustrated in Fig. 5.

To compare the SDAS results, statistical tests (Student's *T*-test) were performed using Microsoft Excel software to compare the base, the center, and the top of the manufactured walls under each condition. At least 12 different fields were measured for SDAS in each condition and position.

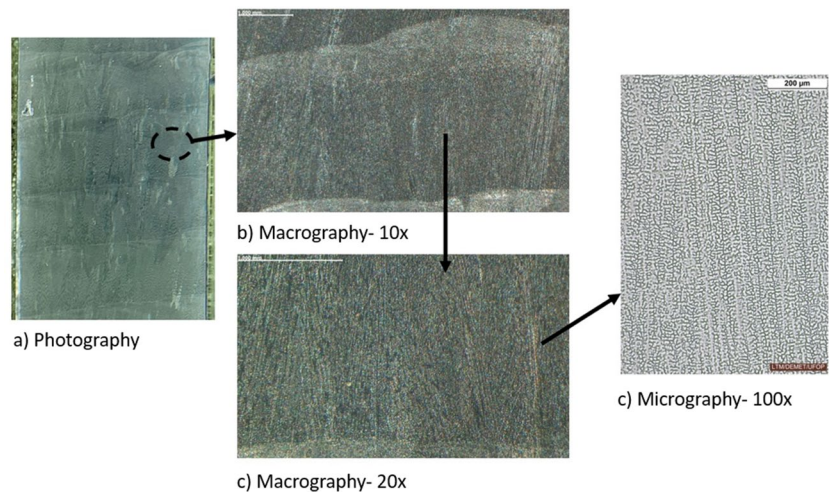
Using the ImageJ software, the volumetric fraction of delta ferrite ( $\delta$ ) present in the walls manufactured by additive manufacturing was estimated. This estimation was based on three fields at different positions at the top of the fabrications.

To evaluate the properties of the walls manufactured by additive manufacturing, Brinell hardness tests were conducted, creating hardness profiles. Specimens extracted from the central region of the manufactured wall were used, and



**Fig. 3** **A** Region designated for metallographic analysis of the walls manufactured by DED-Arc. **B** Locations where thickness measurements were taken on the walls manufactured by additive manufacturing. Points 1 and 3 denote height measurements at the ends, while point 2 represents it at the middle of the wall

**Fig. 4** Representative scheme of the metallographic analysis process. (a) Photograph taken without magnification, (b)  $10\times$  magnification, (c)  $20\times$  magnification, and (d)  $100\times$  magnification performed under the optical microscope. The highlighted region in (a) corresponds to the central position of a layer—metallographic analysis point





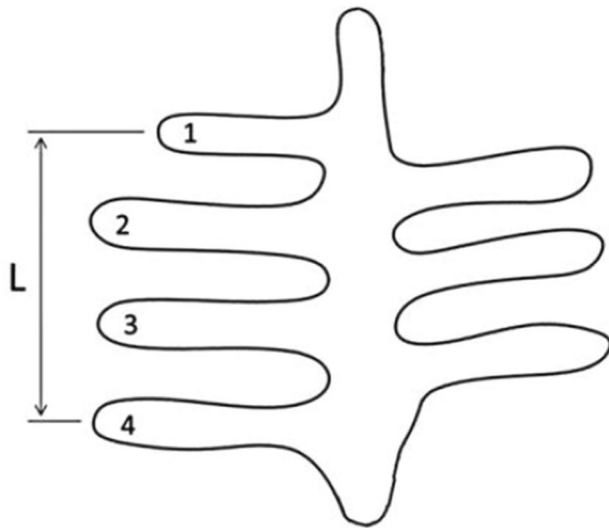


**Fig. 5** Representation of the method to measure the secondary inter-dendritic arm spacing (SDAS) with the lowest associated error [11]. L represents the length parallel to the primary arm, extending from the center of the first dendrite to the center of the last counted dendrite. Vandersluis and Ravindran [11]

hardness profiles were made along the entire height, from the base to the top, with a spacing of 4 mm.

To perform the tensile tests, the specimens were extracted in both the transverse and longitudinal directions of the walls, as shown in Fig. 6.

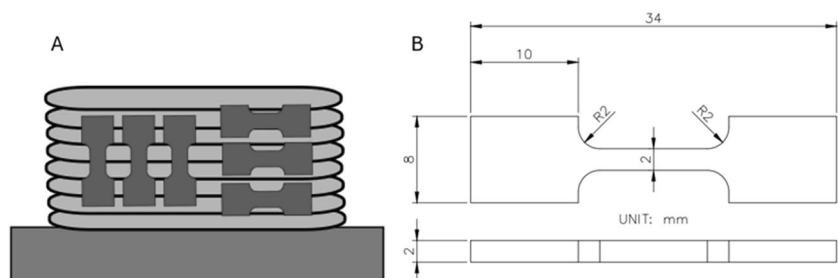
All tests and analyses were conducted comparatively between the two deposition conditions (with and without active cooling). Fractographic analyses were performed on samples from the tensile tests using a scanning electron microscope (SEM).

### 3 Results and discussion

#### 3.1 Manufacturing productivity analysis

The results of the measured times, along with the efficiency of the depositions and productivity increase, are presented in Table 4.

**Fig. 6** A Representation of the sites where the tensile specimens were extracted from the walls manufactured by DED-Arc. B Dimensions of the specimens used in tensile tests



As shown in Table 4, the unidirectional deposition conditions (Air I and NIAC I) exhibited lower efficiency when compared to the bidirectional depositions. This difference is attributed to the torch returning to its initial position without depositing material in unidirectional deposition conditions, which does not happen in bidirectional depositions.

By comparing the conditions using NIAC (cooling tank—NIAC I and NIAC II) with those using natural cooling (Air I and Air II), it is evident that depositions with active cooling exhibit higher efficiency. There is approximately a 22% increase in productivity for unidirectional fabrications and a 108% increase for bidirectional depositions. This improvement is associated with the elimination of idle cooling time during wall construction, owing to reduced heat accumulation.

The increase in efficiency and productivity achieved using the NIAC setup is significant for the DED-Arc field, as it allowed the elimination of the idle cooling time with the studied conditions. As discussed by previous authors [1, 4, 5, 8, 10], idle cooling time is typically employed/required in this process to control heat accumulation, avoid melting collapse, ensure consistent solidification and cooling conditions, and improve the geometry of the manufactured components. According to Reisgen et al. [1], “the manufacturing speed is mainly defined by the deposition rate of the welding process and the idle time that is necessary to let the workpiece cool down to the required interpass temperature.” As will be shown in the following sections, NIAC not only improved productivity but also was effective in enhancing the geometry and microstructure of the deposited material.

**Table 4** Comparison between wall manufacturing time, actual deposition time, and efficiency among the four proposed deposition conditions

| Condition | Total time (min) | Real-time deposition (min) | Efficiency | Productivity increase with NIAC |
|-----------|------------------|----------------------------|------------|---------------------------------|
| Air I     | 24.2             | 10                         | 41%        | -                               |
| Air II    | 20.7             | 10                         | 48%        | -                               |
| NIAC I    | 20.0             | 10                         | 50%        | 22%                             |
| NIAC II   | 10.0             | 10                         | 100%       | 108%                            |

### 3.2 Analysis of the geometry of the specimens

Figure 7 shows the undulations on the fabricated walls, inherent to the layer-by-layer deposition process that was titled “stair-step” [12]. The depositions that employed active cooling (Fig. 7C and D) exhibited higher surface regularity and reduced undulations (due to the *stair-step effect*), as also identified by Silva et al. [7].

The mean height values at the right and left extremities, as well as at the central part of the manufactured walls, were measured using a caliper (Fig. 8). It is possible to verify that, generally, the highest central heights were identified in the depositions that utilized NIAC. This can be attributed to better thermal control. As will be shown,

the thickness of preforms obtained with active cooling was more uniform along their height, similar to previous results [7]. In other words, heat accumulation in naturally cooled conditions increased the size of the melt pool, resulting in greater thickness and, consequently, lower height.

For unidirectional depositions, as seen in Fig. 7A and C, the preforms exhibited an inclination from the left end (the start of the welding pass for each unidirectional deposition) to the right end (the end of the welding pass/arc). As discussed by Hu et al. [13], this significant variation in height accumulates layer by layer and is attributed to differences in the molten pool dynamics at the beginning and end of the electric arc. This effect can explain the results depicted in Fig. 7A and Fig. 8A and is similar to findings by Hu et al.

**Fig. 7** Preforms obtained by DED-Arc using AISI 316LSi in different conditions: **A** Air I—unidirectional and natural cooling; **B** Air II—bidirectional and natural cooling; **C** NIAC I—near immersion active cooling unidirectional; **D** NIAC II—near immersion active cooling bidirectional

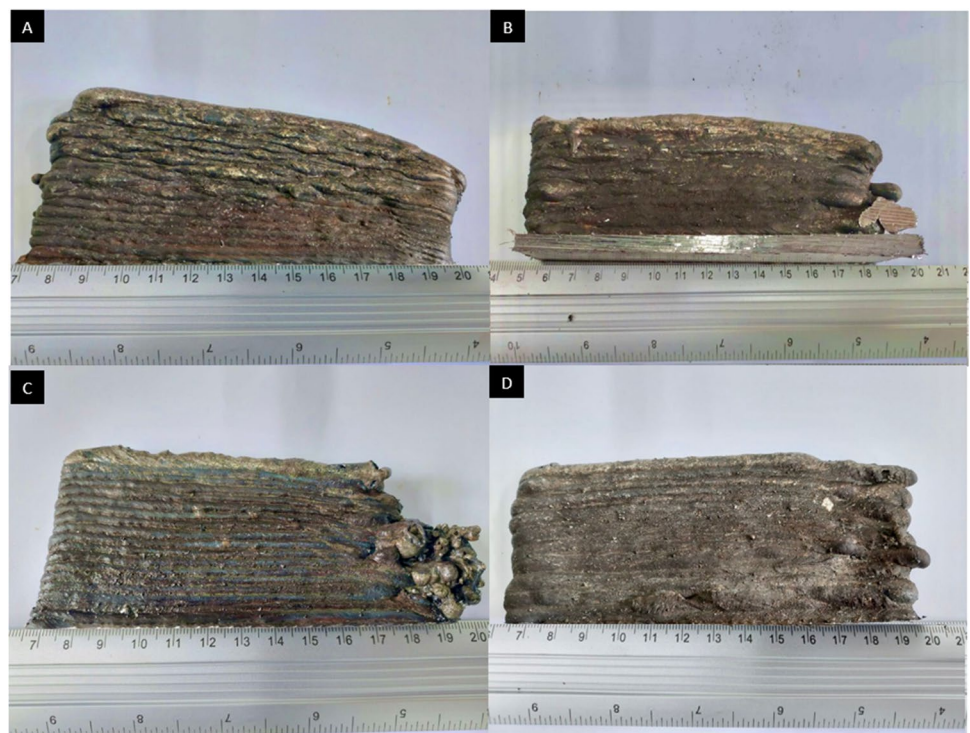
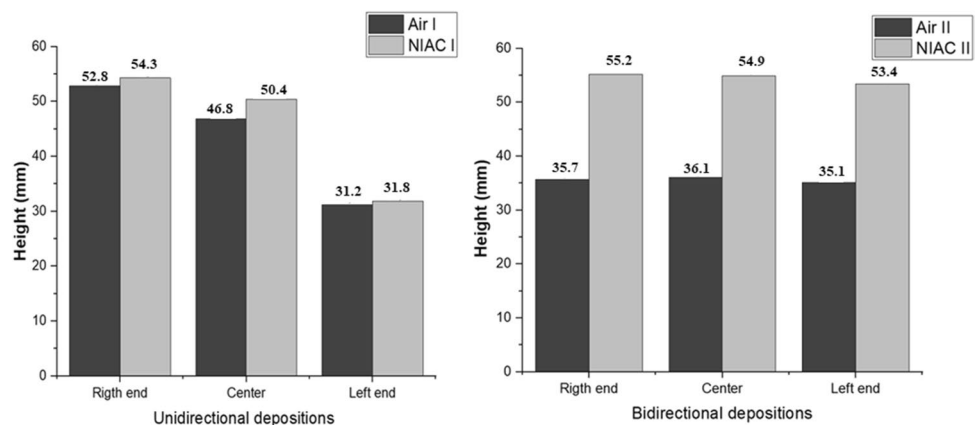


**Fig. 8** Heights of the walls manufactured by **A** unidirectional depositions with and without active cooling and **B** bidirectional depositions with and without active cooling (mm)



[13] using GMAW in unidirectional depositions with an AWS ER70S-6 electrode.

The results obtained in Fig. 7C and the sharp differences in height at the right end of the NIAC I condition (Fig. 8A) can also be explained by the “abnormity at start and end of the weld bead in additive manufacturing with GMAW,” discussed by Hu et al. [13]. However, in this case, due to the presence of water during the deposition, the reduction in the preform height led to contact between the wire/arc and the cooling liquid during the experiments. This occurred because the movement of the welding torch in the vertical axis and the increase in the water level were constant throughout the depositions. As can be seen at the right end of the preform (Fig. 7C), there was a collapse of the welding arc and the molten pool due to their contact with water.

The adoption of bidirectional depositions improved the height consistency along the preforms, as seen in Fig. 7B and D and Fig. 8B. This result was also observed previously [13], where the alternance of the start and end of the welding pool from each consecutive layer counterbalanced the differences in height. Considering the bidirectional deposition path, the collapse of the welding arc/pool due to its contact with the water was avoided, as can be seen in Fig. 7D.

Additionally, it is relevant to highlight that the condition without active cooling and bidirectional deposition, Air II, presented the lowest height values, as shown in Fig. 8B. There was a difference of 18.8 mm in the central position compared to the deposition with active cooling. This is probably related to the excessive heat accumulation during the manufacturing process. This phenomenon was also evidenced in studies conducted by Xu et al. [14], which found the highest temperatures during bidirectional depositions along the entire deposited layer.

Analogous to height measurements, thicknesses were measured at three points: extremities and center, in the top and bottom regions of the thin walls (see Fig. 3). The mean values found for each deposition condition are shown in Table 5.

Table 5 shows that, in general, the depositions with active cooling produced layers of lower thickness, both at the base and at the top of the walls, compared to those without active cooling. Similar results were found in studies by Wu et al. [15], where a considerable increase in the width of the layers along the growth of the preforms was observed when analyzing a cross-section. This was attributed to the impact of heat accumulation on the depositions without active cooling.

Overall, the depositions that adopted NIAC were characterized by higher heights in the center of the manufactured walls and lower thickness, both at the top and bottom of the wall. These findings suggest that the quality of the geometry of walls manufactured with AM can be improved by adopting active cooling by near immersion, especially when considering a bidirectional deposition path.

**Table 5** Average thicknesses measured in the preforms at the center, right-end, and left-end positions at the top and bottom of the four proposed deposition conditions

| Condition | Deposition Path | Top (mm) | Base (mm) |
|-----------|-----------------|----------|-----------|
| Air I     | Unidirectional  | 13.13    | 13.73     |
| Air II    | Bidirectional   | 12.93    | 13.40     |
| NIAC I    | Unidirectional  | 8.97     | 9.77      |
| NIAC II   | Bidirectional   | 9.13     | 9.67      |

### 3.3 Microstructural characterization

The microstructural analyses revealed, in general, how heterogeneous the microstructure is, typical of this type of manufacturing. Figure 9(c) shows fine dendrite lines in the remelting zones and a coarser dendritic zone, consistent with findings reported by Cunningham et al. [8] and Wang et al. [16].

In images at 200× magnification, delta ferrite ( $\delta$ ) is identifiable by its gray color distributed within the austenite matrix ( $\gamma$ ), which appears white (Fig. 10). Defects such as macroporosity and cracks were not found on the surfaces presented, but it is possible to identify the secondary interdendritic arms.

Grains are observed to have grown along the vertical direction of the deposited walls, as indicated by the deposition direction shown in the lower right corner of Fig. 10. Upon comparing the presented micrographs, a seemingly more refined microstructure is observed under conditions that adopted active cooling, which will be further confirmed by quantitative metallography in the next section.

According to Lippold and Kotecki [17], when thermally processed, austenitic stainless steels typically exhibit microstructure that is either completely austenitic or a mixture of austenite and ferrite. The delta ferrite observed in the microstructures in this work is classified as high-temperature residual ferrite.

Ferrite morphology ( $\delta$ ) depends on both solidification and post-solidification transformations, with vermicular and lath structures being the most common for austenitic stainless steels [18].

### 3.4 Secondary interdendritic spacing calculation

To calculate the secondary interdendritic arm spacing, images at 200× magnification were analyzed using ImageJ software. Figure 11 compares the average secondary interdendritic arm spacing found at the base, center, and top of both unidirectional and bidirectional depositions, with and without active cooling.

Figure 11A shows that the highest values of secondary interdendritic arm spacing in unidirectional depositions



were observed in the condition without active cooling (Air I), which confirms that the use of the water tank (NIAC) resulted in a refined microstructure. This effect is attributed to a higher cooling rate in depositions that adopted NIAC, leading to a finer microstructure and a higher amount of

ferrite ( $\delta$ ). Similar observations were reported in the studies by Santos [19] and Silva et al. [7].

In Fig. 11B, the highest values of secondary interdendritic arm spacing were similarly observed in deposition without active cooling, showing a significant difference of

**Fig. 9** Central regions of the thin walls manufactured by additive manufacturing in which the specimens for metallographic analysis were obtained (a). The chosen area aims to avoid reheated regions, focusing on analyzing the center of the layers

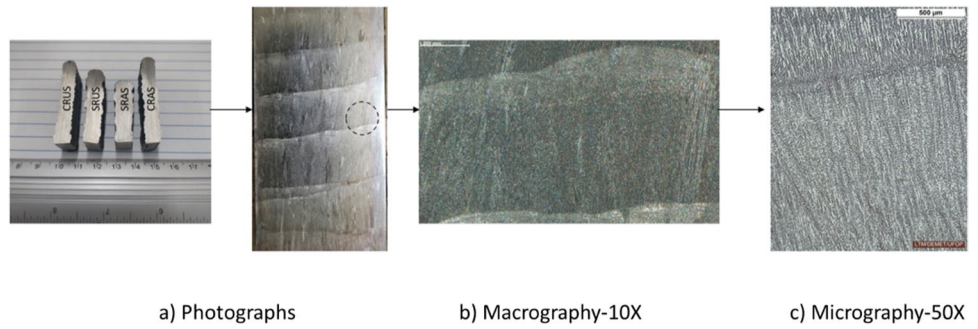


**Fig. 10** Optical micrographs taken in the central region of the manufactured preforms (thin walls) using 200× magnification. Conditions: **A** Air I, **B** NIAC I, **C** Air II, and **D** NIAC II

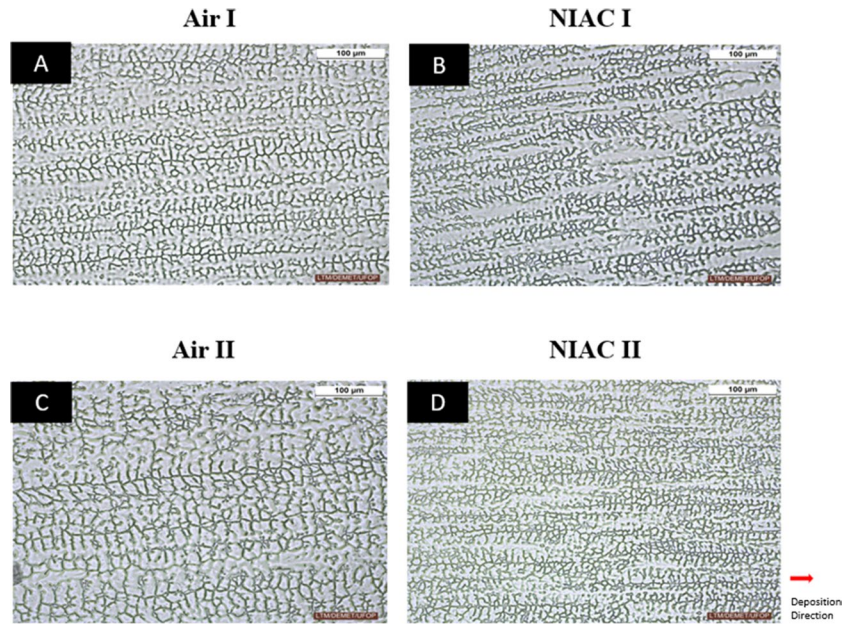
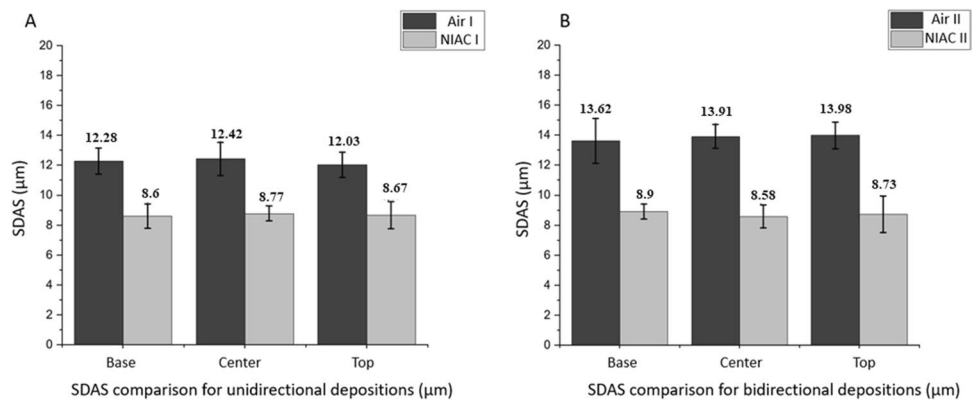


**Fig. 11** Averages of secondary interdendritic arm spacing obtained at the base, center, and top of walls manufactured by unidirectional (A) and bidirectional (B) depositions with and without active cooling





up to 5.36  $\mu\text{m}$  (38%) when comparing the averages found at the tops of thin walls manufactured with a bidirectional path.

It is also important to highlight that, when comparing Fig. 11A and B, it is possible to notice that the average SDAS observed in walls manufactured via bidirectional deposition, with and without active cooling, were higher than those measured in unidirectional depositions. This outcome is associated with a lower cooling rate in bidirectional depositions. Unlike unidirectional depositions, bidirectional ones do not pause deposition at the ends of the manufactured wall to return the torch to the initial position.

Therefore, in bidirectional depositions, there is less time for cooling, resulting in more heat accumulation in the wall. The variations in primary and secondary dendritic spacings are influenced by solidification thermal conditions such as cooling rate and solidification front growth rate, as evidenced in studies by Antonello [20]. These factors contribute to the differences observed in the SDAS between unidirectional and bidirectional depositions.

Statistical tests (Student’s *T*-test) were performed to compare the mean SDAS found in the centers of the thin walls manufactured in each condition. The results of Student’s *T*-tests for unidirectional and bidirectional depositions confirmed significant differences between the microstructures. This underscores, statistically, the effects of active cooling on the microstructures of manufactured walls in both types of deposition strategies.

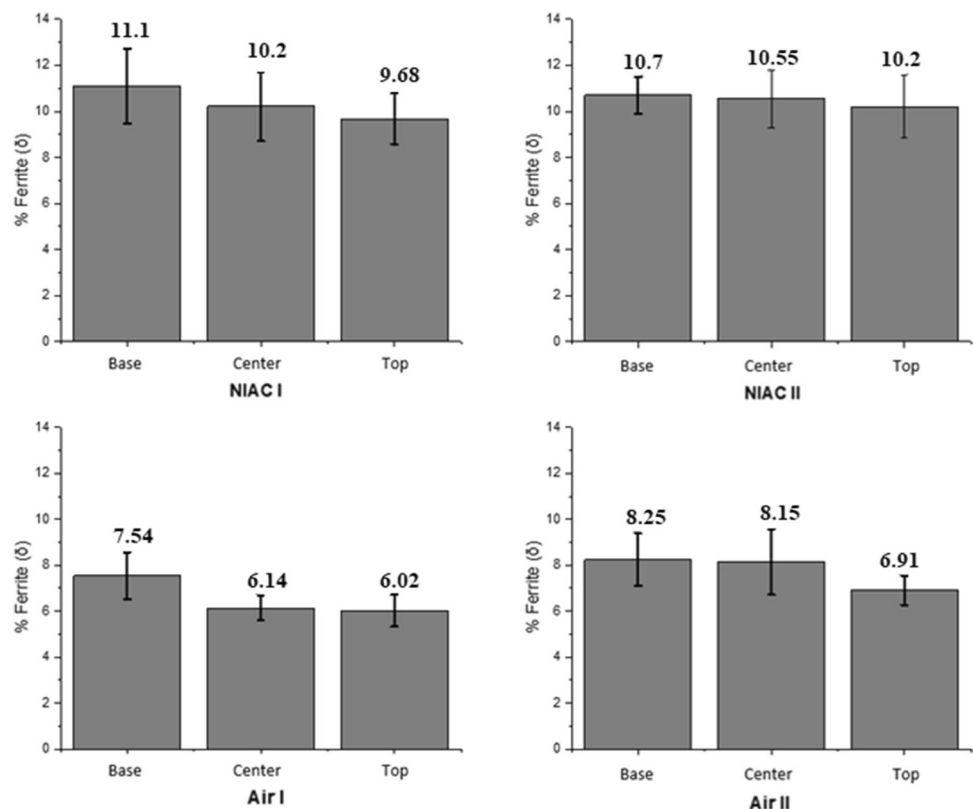
In addition to analyzing secondary interdendritic arm spacing, the volume fraction of delta ferrite ( $\delta$ ) was calculated using ImageJ (Fig. 12). The results indicate that conditions employing NIAC exhibited a significantly higher volumetric fraction of ferrite ( $\delta$ ) compared to walls manufactured without active cooling.

The percentage of ferrite ( $\delta$ ) found in the four deposition conditions was consistent with the range estimated by Pessanha [21], which varies from 5 to 20% of ferrite in cast austenitic stainless steels. Furthermore, the ranges of ferrite volume fraction ( $\delta$ ) found were similar to those reported by Souza [6], who also used ImageJ to estimate the volumetric fraction of this constituent in AISI 316L steel tubes obtained by DED-Arc.

The increase in the ferrite fraction ( $\delta$ ) observed in conditions with active cooling can be attributed to the higher cooling rates resulting from the NIAC technique [9]. The results are consistent with the SDAS values found, since there was an increase in the volume fraction of ferrite in the conditions that adopted NIAC.

In general, for conditions without active cooling, similar to what was reported by Jafarzad-Shayan et al. [9], the highest volumetric fractions of ferrite ( $\delta$ ) were found in the region at the base of the preforms (Fig. 12). This result is related to the higher heat transfer with the base on which the thin walls were built. In contrast, the central region displayed intermediate ferrite fractions, while the top showed

**Fig. 12** Volumetric fraction of delta ferrite identified in micrographs obtained at the base, center, and top of walls manufactured by additive manufacturing in the four evaluated conditions



lower values, indicative of reduced cooling rates attributed to heat accumulation as the height of the wall increases. The difference was more pronounced in the conditions without active cooling.

### 3.5 Brinell hardness tests

From Brinell hardness tests (Fig. 13), an average difference of 13 HB was observed between bidirectional conditions using NIAC and natural cooling. In the case of the unidirectional path, the average difference increased to 20 HB.

It is important to highlight that the observed hardness values in walls manufactured with active cooling were consistently higher than those in walls manufactured with natural cooling, regardless of deposition direction (in one and both directions). This trend may be linked to the finer microstructure achieved in depositions with NIAC, which is associated with a higher cooling rate during these fabrications, as highlighted by Michla et al. [22]. This refinement is supported

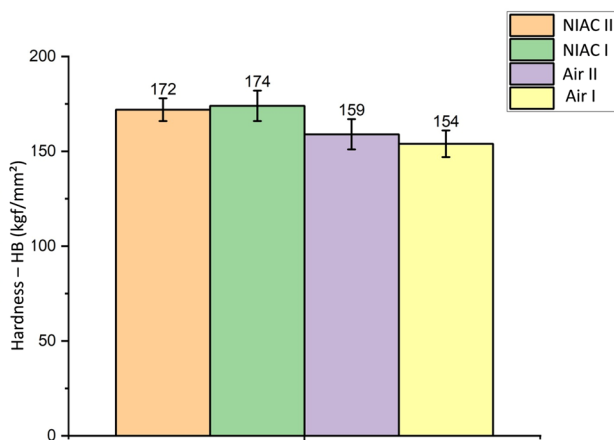
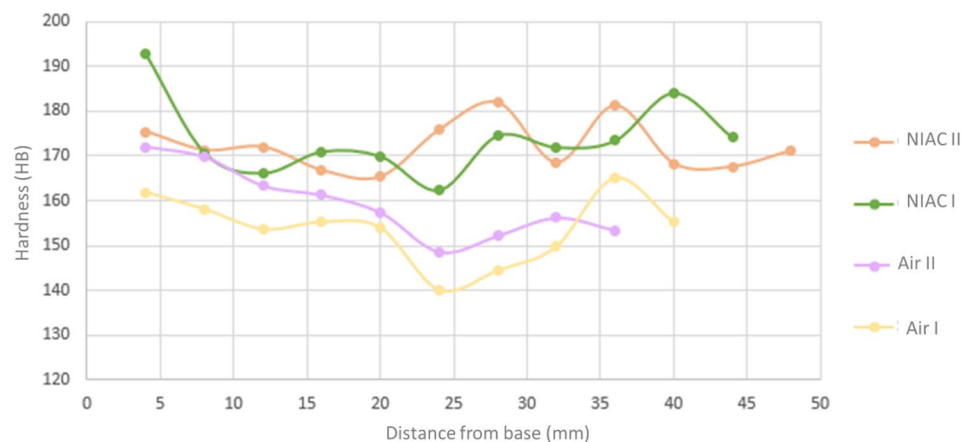


**Fig. 13** Brinell hardness values obtained in samples extracted from thin walls manufactured under the four evaluated conditions: NIAC (I and II) and Air (I and II)

**Fig. 14** Hardness profiles along the height of walls manufactured according to different patch/cooling conditions: Air (I and II), NIAC (I and II)



by the SDAS measurements shown in Fig. 11. Additionally, the increased presence of ferrite ( $\delta$ ), as noted in studies by Ghasemi et al. [23], may contribute to the higher average hardness observed in the manufactured walls.

Furthermore, a hardness profile was carried out along the height of the preforms manufactured under the evaluated deposition conditions, depicted in Fig. 14. The profile was made from the base to the top, with 4 mm of distance between the indentations. The starting point of the profile corresponds to the material near the base, marked as 0 in Fig. 14.

It is possible to conclude that, although the standard deviation is quite similar for all depositions, a dispersion in hardness values was observed along the height of the walls. It is important to note that, unlike the procedure adopted in quantitative metallographic analyses, it was not possible to guarantee that the hardness indentations were carried out in more uniform regions of the layers. In other words, there is macrostructural heterogeneity throughout the height of the deposited walls, as discussed by Cunningham et al. [8]. Thus, the dispersion in hardness along the height can be associated with these microstructural variations.

### 3.6 Tensile tests

To conduct the tensile tests, specimens were extracted in both the transverse and longitudinal directions. Figure 15 illustrates that, overall, the yield strength of samples manufactured with active cooling was higher compared to those in walls manufactured with natural (air) cooling, except for the longitudinal unidirectional condition, in which the standard deviation was also notably higher.

One of the factors responsible for the increase in yield strength in parts manufactured using NIAC may be the reduction in secondary interdendritic arm spacing. Studies conducted by Sander et al. [24], Zhang et al. [25], and Godec et al. [26] have highlighted the direct influence of this variable on the yield strength of 316L stainless steel.

This is due to the greater number of grain boundaries, which tend to difficult dislocation motion, resulting in increased mechanical strength.

It is possible to observe that across all four deposition conditions, the tensile test specimens obtained from walls manufactured with active cooling exhibited lower elongation values compared to those obtained with natural cooling.

In the work of Wang et al. [16], the authors highlighted the influence of the heterogeneities in the microstructures obtained by AM of AISI 316L steel. They found that in the remelting lines, which presented more refined structures and dendritic growth perpendicular to the tensile test direction, there were limitations in the expansion of the slip bands. As a result, this direction exhibited lower elongation and greater tensile strength due to the directional growth of the dendrites.

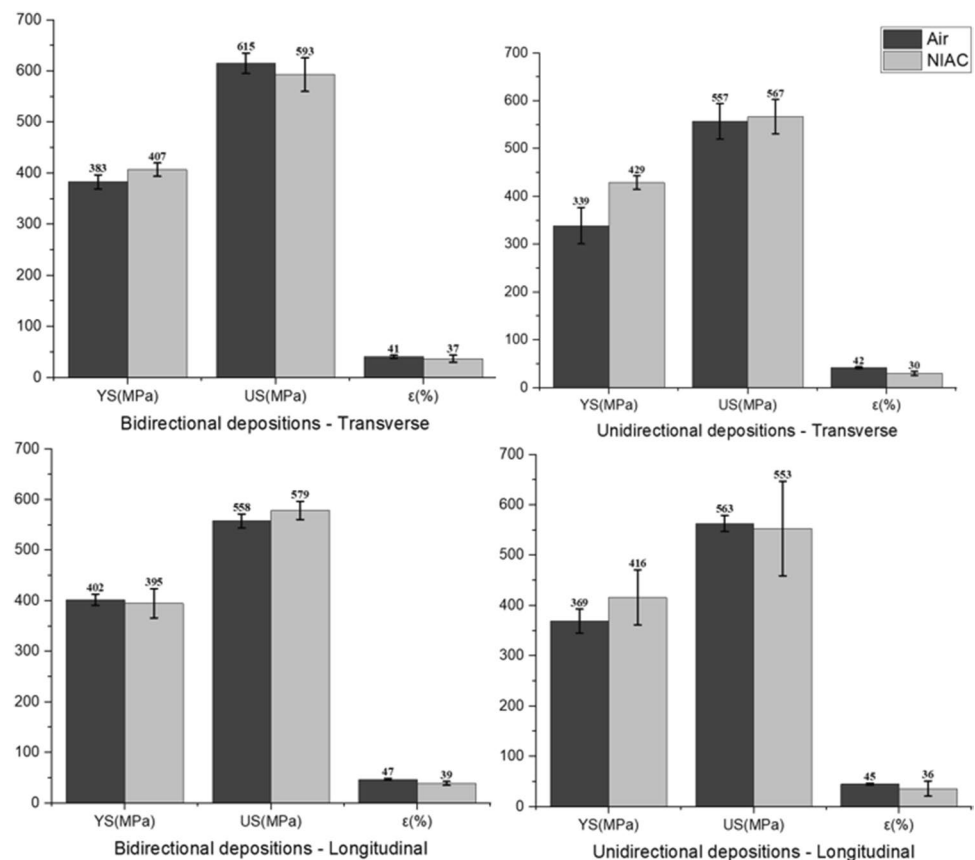
Furthermore, it is worth noting that the highest elongation values were achieved under manufacturing conditions that employed air cooling. Wu et al. [27] observed a similar trend in their research when depositing thin walls of AISI 316L. In their study, the authors analyzed the grain morphology fracture surfaces and found that during tensile testing in the longitudinal direction, fracture occurred after enlargement of the deformed columnar grains. In contrast, during tensile test in the transverse direction, there was minimal grain

deformation, and the boundaries of the columnar grains proved to be the weakest points in the tensile process. Consequently, the sample with a greater number of grain boundaries in the longitudinal direction exhibited lower tensile strength compared to the sample in the transverse direction.

Finally, it is important to note that the values obtained from the tensile tests were consistent with the literature, such as reported by Koppu et al. [28], for natural (air) cooling conditions. The low elongation values observed in unidirectional depositions employing active cooling can be attributed to material heterogeneity, the presence of discontinuities, and difficulties in maintaining consistent water levels, which led to porosity issues, as will be detailed in the next section. Due to the geometric effects observed in Fig. 7C, which resulted in contact between the arc/pool and water at the right end, unidirectional depositions with NIAC exhibited higher levels of water vapor in the arc atmosphere. This could explain the presence of pores observed on the fracture surfaces of samples from this condition.

Furthermore, a comprehensive comparison between the mean yield strength, ultimate tensile strength, and elongation in the longitudinal and transverse directions to assess potential anisotropies could not be fully conducted. As will be presented in the next section, some specimens exhibited typical AM discontinuities on their fracture surfaces, such

**Fig. 15** Comparison between yield strength (YS), ultimate tensile strength (US), and elongation ( $\epsilon$ ) obtained in the tensile tests of the specimens extracted from walls manufactured by AM in the longitudinal and transverse directions for the four evaluated deposition conditions



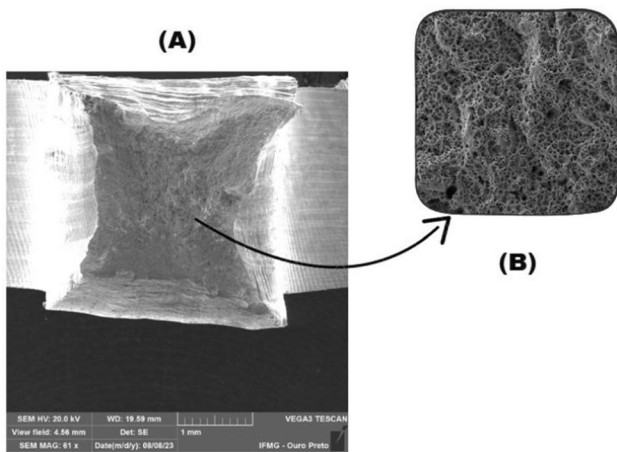


**Fig. 16** Fracture surface of a tensile specimen extracted from a wall manufactured via additive manufacturing in condition Air II, in the transverse direction. Enlarged **A** 60 $\times$  and **B** 1000 $\times$

as lack of fusion and porosity. Therefore, the properties measured in tensile tests are not only due to microstructural variations resulting from different cooling conditions and deposition path/directions, but also by these inherent AM discontinuities.

### 3.7 Fractographic analysis

After conducting the tensile tests, the fractured surfaces underwent analysis using a scanning electron microscope (SEM). Figure 16 illustrates a fracture surface from a specimen extracted from a wall manufactured via additive manufacturing with bidirectional deposition and natural (air) cooling (Air II).

All samples from this condition exhibited ductile fracture characteristics, prominently displaying dimples across the surface, as depicted in Fig. 16B. The presence of extensive plastic deformation is also evident, characteristic of AISI 316L stainless steel, which has high ductility, as noted by Cunningham et al. [8] and Michla et al. [22].

Some samples from conditions employing the NIAC technique exhibited discontinuities, many of which were characterized by lack of fusion or formation of porosities. These issues are primarily attributed to challenges in controlling the water level, resulting in water vapor in the arc atmosphere. The surfaces of these discontinuities revealed the presence of dendritic-like structures (Fig. 17), which are typical features of the solidification process, as reported by Santos [3] and Wang et al. [19].

Additionally, outside the regions affected by discontinuities, the fracture exhibited a ductile appearance characterized by the presence of dimples. Figure 17 illustrates the fractographic analysis of a tensile sample from the NIAC I condition.

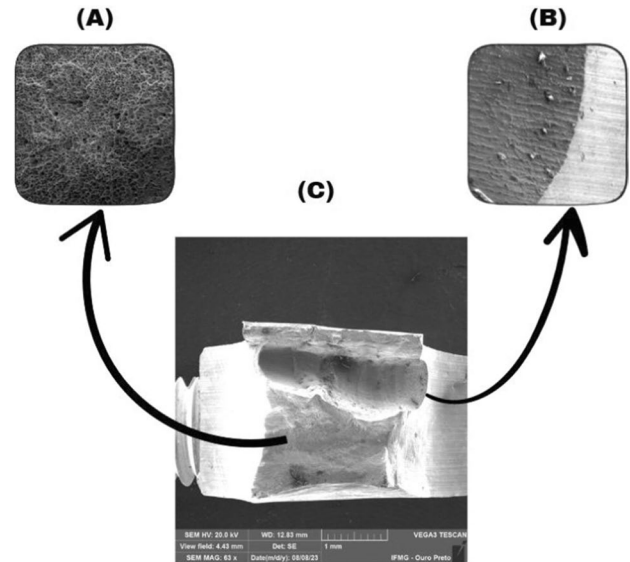


**Fig. 17** Fracture surface of a tensile test specimen from the NIAC I condition in the longitudinal direction. Enlargement by **A** 1000 $\times$ , **B** 500 $\times$ , and **C** 60 $\times$ . Highlighted in **B** is the surface of a discontinuity, with dendritic-like structures

As observed in Fig. 17, the fracture occurred in a region containing a discontinuity, due to stress concentration. The effect of porosities was also noticeable in the results available in Fig. 15, in which it is evident that the NIAC I condition—in the longitudinal direction exhibits a higher standard deviation compared to other conditions using active cooling.

## 4 Conclusions

The present study investigated four deposition conditions for manufacturing preforms using WAAM with AISI 316LSi: natural (air) cooling with unidirectional and bidirectional depositions, and near immersion active cooling (NIAC) with unidirectional and bidirectional depositions.

After comparative analysis by microstructural characterization, hardness tests, tensile tests, and fractographic analysis, it was possible to conclude that:

- The adoption of NIAC significantly improved thermal control during the deposition process, as evidenced by more uniform heights and reduced thickness of the manufactured walls compared to natural cooling conditions.
- The elimination of idle cooling time in the NIAC setup enhanced productivity efficiency by up to 108% by preventing excessive heat accumulation and ensuring a more consistent solidification and cooling condition.
- Microstructural analysis revealed that NIAC resulted in a finer microstructure with higher amounts of delta ferrite due to increased cooling rates. This was supported by the



SDAS measurements, which were lower by up to 38% in the NIAC conditions.

- The adoption of the NIAC technique resulted in an approximately 10% increase in hardness. Additionally, tensile tests indicated an increase in mechanical strength, especially in yield strength, attributed to the lower secondary interdendritic spacing, although a reduction in ductility was observed.
- Fracture analysis of tensile samples revealed ductile characteristics in air-cooled conditions, while some NIAC samples showed discontinuities due to water vapor in the arc atmosphere.
- Finally, it is important to highlight that the NIAC technique proved to be promising for temperature control, increasing productivity, microstructural conditioning, and improving the mechanical strength of AISI 316LSi steel obtained by DED-Arc.

**Funding** This work was supported by the Coordenação de Aperfeiçoamento de Pessoal de Nível Superior (CAPES) and Fundação de Amparo à Pesquisa de Minas Gerais (FAPEMIG).

**Data availability** Not applicable.

**Code availability** Not applicable.

## Declarations

**Ethics approval** Not applicable.

**Consent to participate** All authors read and approved the final manuscript.

**Consent for publication** All authors agree to publish in *The International Journal of Advanced Manufacturing Technology*.

**Conflict of interest** The authors declare no competing interests.

## References

1. Reisgen U, Sharma R, Mann S, Oster L (2020) Increasing the manufacturing efficiency of WAAM by advanced cooling strategies. *Welding in the World* 64(8):1409–1416. <https://doi.org/10.1007/s40194-020-00930-2>
2. ISO/ASTM (2021) 52900. Additive manufacturing—General principles—Fundamentals and vocabulary: ISO/ASTM International. p. 12.
3. Wang L, Xue J, Wang Q (2019) Correlation between arc mode, microstructure, and mechanical properties during wire arc additive manufacturing of 316L stainless steel. *Mater Sci Eng, A* 751:183–190. <https://doi.org/10.1016/j.msea.2019.02.078>
4. Wu W, Xue J, Wang L, Zhang Z, Hu Y, Dong C (2019) Forming Process, microstructure, and mechanical properties of thin-walled 316L stainless steel using speed-cold-welding additive manufacturing. *Metals*. <https://doi.org/10.3390/met9010109>
5. da Silva LJ, Souza DM, de Araújo DB, Reis RP, Scotti A (2020) Concept and validation of an active cooling technique to mitigate heat accumulation in WAAM. *The International Journal of Advanced Manufacturing Technology* 107(5):2513–2523. <https://doi.org/10.1007/s00170-020-05201-4>
6. Souza LBOd (2022). Correlação entre processos de fabricação convencional e por manufatura aditiva com as propriedades do aço inoxidável 316L. Dissertation, Universidade Federal de Uberlândia. <https://doi.org/10.14393/ufu.di.2022.82>
7. Silva L (2019). Near-immersion active cooling for wire + arc additive manufacturing: from concept to application. Thesis, Universidade Federal de Uberlândia. <https://doi.org/10.14393/ufu.te.2019.2422>
8. Cunningham C, Wang J, Dhokia V, Shokrani A, Newman S (2019) Characterisation of austenitic 316LSi stainless steel produced by wire arc additive manufacturing with interlayer cooling. In: Proceedings of the 30th annual international solid freeform fabrication symposium. University of Texas Austin, pp 426–439. <http://dx.doi.org/10.26153/tsw/17282>
9. Jafarzad-Shayan MM et al (2023) Microstructural heterogeneity and exceptional mechanical properties in a wire-arc additively manufactured stainless steel. *Mater Sci Eng, A* 882:145473. <https://doi.org/10.1016/j.msea.2023.145473>
10. Jin W, Zhang C, Jin S, Tian Y, Wellmann D, Liu W (2020) Wire arc additive manufacturing of stainless steels: a review. *Appl Sci*. <https://doi.org/10.3390/app10051563>
11. Vandersluis E, Ravindran C (2017) Comparison of Measurement Methods for Secondary Dendrite Arm Spacing. *Metallogr Microstruct and Anal* 6(1):89–94. <https://doi.org/10.1007/s13632-016-0331-8>
12. Xiong J, Zhang G (2014) Adaptive control of deposited height in GMAW-based layer additive manufacturing. *J Mater Process Technol* 214(4):962–968. <https://doi.org/10.1016/j.jmatprotec.2013.11.014>
13. Hu Z, Qin X, Shao T, Liu H (2018) Understanding and overcoming of abnormality at start and end of the weld bead in additive manufacturing with GMAW. *Int J Adv Manuf Technol* 95(5):2357–2368. <https://doi.org/10.1007/s00170-017-1392-9>
14. Xu T, Liu J et al (2023) Fabrication strategy and macroscopic defect control of large-size component based on double-wire arc additive manufacturing. *Int J Adv Manuf Technol* 125(5):2609–25. <https://doi.org/10.1007/s00170-023-10882-8>
15. Wu B, Pan Z et al (2018) A review of the wire arc additive manufacturing of metals: properties, defects and quality improvement. *J Manuf Process* 35:127–139. <https://doi.org/10.1016/j.jmapro.2018.08.001>
16. Wang C, Liu TG, Zhu P, Lu YH, Shoji T (2020) Study on microstructure and tensile properties of 316L stainless steel fabricated by CMT wire and arc additive manufacturing. *Mater Sci Eng, A* 796:140006. <https://doi.org/10.1016/j.msea.2020.140006>
17. Lippold JC, Kotecki DJ (2005) *Welding metallurgy and weldability of stainless steels*. John Wiley & Sons, Hoboken, New Jersey
18. Palmeira Belotti L, van Dommelen JAW, Geers MGD, Goulas C, Ya W, Hoefnagels JPM (2022) Microstructural characterisation of thick-walled wire arc additively manufactured stainless steel. *J Mater Process Technol* 299:117373. <https://doi.org/10.1016/j.jmatprotec.2021.117373>
19. Santos EP (2017) Estudo comparativo das transformações microestruturais e termometalúrgicas de juntas soldadas dos aços inoxidáveis AISI 316 e AISI 316L pelos processo TIG autógeno. Dissertation, Universidade Federal Fluminense
20. Antonello MG (2022) Construção e expansão eletromagnética do arco elétrico no processo GTAW aplicada na manufatura aditiva. Thesis, Universidade Federal de Minas Gerais.
21. Pessanha EC (2011). Quantificação da ferrita delta e avaliação da relação microestrutura/propriedades de um aço inoxidável

- austenítico 347 soldado. Dissertation, Universidade Estadual do Norte Fluminense Darcy Ribeiro
22. Michla JRJ, Nagarajan R, Krishnasamy S, Siengchin S, Ismail SO, Prabhu TR (2021) Conventional and Additively Manufactured Stainless Steels: A Review. *Trans Indian Inst Met* 74(6):1261–1278. <https://doi.org/10.1007/s12666-021-02305-7>
  23. Ghasemi R, Beidokhti B, Fazel-Najafabadi M (2023) Effect Of Delta Ferrite On The Mechanical Properties Of Dissimilar Ferritic-Austenitic Stainless Steel Welds. *Arch Metall Mater.* 63:437–443. <https://doi.org/10.24425/118958>
  24. Sander G, Babu AP, Gao X, Jiang D, Birbilis N (2021) On the effect of build orientation and residual stress on the corrosion of 316L stainless steel prepared by selective laser melting. *Corros Sci* 2021(179):109149. <https://doi.org/10.1016/j.corsci.2020.109149>
  25. Zhang K, Wang S, Liu W, Shang X (2014) Characterization of stainless steel parts by Laser Metal Deposition Shaping. *Mater Des* 55:104–119. <https://doi.org/10.1016/j.matdes.2013.09.006>
  26. Godec M, Zaefferer S, Podgornik B, Šinko M, Tchernychova E (2020) Quantitative multiscale correlative microstructure analysis of additive manufacturing of stainless steel 316L processed by selective laser melting. *Mater Charact* 160:110074. <https://doi.org/10.1016/j.matchar.2019.110074>
  27. Wu B, Pan Z, Ding D, Cuiuri D, Li H, Fei Z (2018) The effects of forced interpass cooling on the material properties of wire arc additively manufactured Ti6Al4V alloy. *J Mater Process Technol* 258:97–105. <https://doi.org/10.1016/j.jmatprotec.2018.03.024>
  28. Koppu AK, Lautre NK, Motwani A, Puri Y (2023) Mechanical and Microstructure Investigation of TiC-inoculated SS316LSi Thin Wall Deposited by CMT-WAAM. *Trans Indian Inst Met* 76(8):2307–2314. <https://doi.org/10.1007/s12666-023-02943-z>

**Publisher's note** Springer Nature remains neutral with regard to jurisdictional claims in published maps and institutional affiliations.

Springer Nature or its licensor (e.g. a society or other partner) holds exclusive rights to this article under a publishing agreement with the author(s) or other rightsholder(s); author self-archiving of the accepted manuscript version of this article is solely governed by the terms of such publishing agreement and applicable law.